

# The impulsive phase of magnetar giant flares: assessing linear tearing as the trigger mechanism

C. Elenbaas<sup>1\*</sup>, A. L. Watts<sup>1</sup>, R. Turolla<sup>2,3</sup>, J. S. Heyl<sup>4</sup>

<sup>1</sup>*Anton Pannekoek Institute for Astronomy, University of Amsterdam, Science Park 904, 1098XH, Amsterdam, The Netherlands.*

<sup>2</sup>*Department of Physics and Astronomy, University of Padova, via Marzolo 8, 35131, Padova, Italy.*

<sup>3</sup>*Mullard Space Science Laboratory, University College London, Holbury St. Mary, Surrey, RH5 6NT, UK .*

<sup>4</sup>*University of British Columbia, Vancouver, Canada.*

8 November 2021

## ABSTRACT

Giant  $\gamma$ -ray flares comprise the most extreme radiation events observed from magnetars. Developing on (sub)millisecond timescales and generating vast amounts of energy within a fraction of a second, the initial phase of these extraordinary bursts present a significant challenge for candidate trigger mechanisms. Here we assess and critically analyse the linear growth of the relativistic tearing instability in a globally twisted magnetosphere as the trigger mechanism for giant  $\gamma$ -ray flares. Our main constraints are given by the observed emission timescales, the energy output of the giant flare spike, and inferred dipolar magnetic field strengths. We find that the minimum growth time of the linear mode is comparable to the  $e$ -folding rise time, i.e.  $\sim 10^{-1}$  ms. With this result we constrain basic geometric parameters of the current sheet. We also discuss the validity of the presumption that the  $e$ -folding emission timescale may be equated with the growth time of an MHD instability.

**Key words:** stars: magnetars – X-rays: bursts – magnetic reconnection

## 1 INTRODUCTION

Magnetars are neutron stars (NSs) whose output power is dominated by the decay of an ultra-strong magnetic field (often exceeding the quantum critical field,  $B_{\text{qed}} \equiv m_e^2 c^3 / (e\hbar) \simeq 4.41 \times 10^{13}$  G) (Thompson & Duncan 1995, e.g. Mereghetti 2008; Turolla et al. 2015). The transient emission properties of such sources include comparatively minor recurrent soft  $\gamma$ -ray bursts ( $E \lesssim 10^{42}$  erg) and sporadic giant  $\gamma$ -ray flares ( $E \sim 10^{44} - 10^{46}$  erg)<sup>1</sup>. At present, three giant flares have been observed from independent sources and their lightcurves exhibit remarkably similar characteristics (see Figure 2 in Section 2). Giant flares are typically composed of an explosive initial hard  $\gamma$ -ray spike ( $k_B T_{\text{spec}} \sim 175 - 250$  keV) that develops within (sub)milliseconds and lasts a mere fraction of a second ( $\sim 0.15 - 0.5$  s), and a quasi-exponentially abating x-ray tail ( $\sim 20 - 30$  keV) that persists for minutes, with superimposed pulsations (see e.g. Mazets et al. 1979; Fenimore et al. 1996; Hurley et al. 1999; Feroci et al. 2001; Palmer et al. 2005).

The emission of the decaying tail is argued to be the result of a continuously evaporating and locally magnetically

trapped thermal photon-pair fireball. Beamed emission from this moves in and out the line of sight, due to the rotation of the underlying NS (Thompson & Duncan 1995). The physical process behind the onset, the trigger mechanism, that would clarify the impulsive phase of these energetic flares, remains however a topic of great debate. Here we will discuss one such mechanism, spontaneous tearing of a globally extended equatorial current sheet, in more detail. Typical emission timescales of the observed giant flares play a critical role in resolving this dispute.

### 1.1 Giant flare trigger mechanisms

In this section we briefly explore the various magnetar giant flare trigger mechanisms that have been proposed. We begin with the setup of the system prior to the explosive event and proceed with the triggers, subdivided in internal and external mechanisms.

#### 1.1.1 Setup: magnetic field formation and evolution

The origin of the strong magnetic field is a non-trivial affair. Thompson & Duncan (1992) have argued that during the transient phase of extensive neutrino cooling moments after gravitational collapse of the progenitor star, entropy-driven convection and differential rotation inside a rapidly spinning

\* E-mail: C.P.C.Elenbaas@uva.nl

<sup>1</sup> Energy discharge estimates assume an isotropic release of radiation.

(initial spin period:  $\Omega_0^{-1} \sim 1$  ms) proto-NS may sustain an efficient  $\alpha$ - $\Omega$  dynamo which could generate an internal magnetic field up to  $\sim 10^{17}$  G. Alternatively, the massive progenitor may already accommodate a sizeable magnetic field. An ultra-strong field is consequently formed via straightforward flux conservation of the fossil field during implosion (Ferrario & Wickramasinghe 2006).

The dynamical timescale of the newly formed ultra-strong field is only seconds or less, and the crystallisation of the outer layer does not set in for another couple of minutes to hours. This allows the field to evolve readily towards a (meta-)stable magneto-hydrodynamic (MHD) equilibrium configuration, likely consisting of a combination of a poloidal- and toroidal component, before its further evolution is constrained by the presence of a highly conductive solid crust (Flowers & Ruderman 1977; Braithwaite & Spruit 2006). The problem of magnetic-field stability, and the respective strengths of the two field components have been studied by e.g. Braithwaite (2009), Lander & Jones (2012), and Ciolfi & Rezzolla (2013). No consensus has been reached on these matters yet, and further investigations including the effects of superconductivity (Lander 2014; Henriksson & Wasserman 2013) and the NS crust (Gourgouliatos & Cumming 2014) are required to advance the issue. Subsequent evolution of the strongly twisted field is then determined by ambipolar diffusion, Ohmic decay, and (non-diffusive) Hall drift which occur throughout the interior of the NS (crust and core) and operate on much longer timescales  $\gtrsim 10^4$  yr (Thompson & Duncan 1996; Heyl & Kulkarni 1998). The conductive crust either severely resists the imparted motion of the frozen-in magnetic flux tubes such that Maxwell stress builds up continuously in the system or allows for a constrained transport of magnetic helicity into the magnetosphere, which in turn may develop into a sheared configuration. A reservoir of energy grows (internally or externally) until a certain critical threshold is reached, suddenly releasing the energy in an explosive manner through e.g. a crustal failure or MHD instability of the magnetic field.

### 1.1.2 Internal trigger

Motivated by the duration of the impulsive phase ( $\sim 0.1 - 1$  s) Thompson & Duncan (1995) initially proposed an internal trigger mechanism whereby a large-scale interchange instability, i.e. a global MHD rearrangement, would take place in the liquid core of the NS and propagate outward on a dynamical timescale, equal to the internal Alfvén crossing time,

$$\tau_A^{\text{int}} = \frac{R_*}{v_A^{\text{int}}} \sim 0.1 \text{ s}, \quad (1)$$

where  $R_* \sim 10^6$  cm is the typical radius of a NS and  $v_A^{\text{int}} \sim 10^7 B_{15}^{\text{int}} \text{ cm s}^{-1}$  is the core Alfvén speed for a density  $\sim 10^{15} \text{ g cm}^{-3}$  with the core magnetic field strength given by  $B^{\text{int}} \equiv B_{15}^{\text{int}} \times 10^{15} \text{ G}$ . This results in a sudden global displacement of the magnetic footpoints on the surface of the star injecting an ‘Alfvén pulse’ into the magnetosphere, which subsequently induces a relativistic outflow of plasma. The (sub)millisecond rise of the giant flare lightcurve is, they argue, the signature of a reconnection front in the magnetosphere leading the relativistic outflow, which in turn devel-

ops on the external Alfvén crossing time,

$$\tau_A^{\text{ext}} = \frac{R_*}{v_A^{\text{ext}}} \sim 3 \times 10^{-2} \text{ ms}, \quad (2)$$

where  $v_A^{\text{ext}} \sim c$  is the magnetospheric Alfvén speed. Therefore, even though we initially observe the emission from the reconnection front, the trigger nevertheless is given by the onset of the internal instability<sup>2</sup>.

A second trigger mechanism introduced by Thompson & Duncan (2001) involves the force balance between the rigidity of the elastic NS crust and vast magnetic shear-stress, imparted through the anchored magnetic field lines<sup>3</sup>. Ultimately, the tension of the strongly twisted magnetic field in the crust will become the dominant force and drive the crustal lattice beyond its critical straining threshold  $\theta_{\text{crit}}$ . As the crust yields, the suppressed magnetic energy is allegedly liberated abruptly through a propagating fracture – analogous to an earthquake – producing seismic modes, which in turn couple to magnetospheric Alfvén modes via the pinned magnetic field lines (Blaes et al. 1989).

Thompson & Duncan (2001) note however that the storage capacity of elastic energy in the crust

$$E_{\text{elastic}}^{\text{max}} \sim 1.7 \times 10^{43} \left( \frac{\theta_{\text{crit}}}{10^{-2}} \right)^2 \text{ erg}, \quad (3)$$

which depends on its critical yield strain, is insufficient to explain the observed output power of a giant flare ( $E \gtrsim 10^{44}$  erg). Accordingly, they argued that the crust merely functions as a gate that assists in the storage and discharge of the internal magnetic energy, rather than as the main energy reservoir. It is important to remark however that they assumed conservatively  $\theta_{\text{crit}} \lesssim 10^{-2}$ , yet this value has since been revised by Horowitz & Kadau (2009) through molecular dynamics simulations to be  $\theta_{\text{crit}} \sim 0.1$  (this value has been independently reproduced by Hoffman & Heyl 2012). With this we obtain  $E_{\text{elastic}}^{\text{max}} \sim 10^{45}$  erg [see Eq. (3)], which is comparable to the total energy output of the giant flares. Note however that the value for the critical breaking strain decreases significantly, due to defects induced in the crust after the first time it yields (Hoffman & Heyl 2012). Nonetheless, Lander et al. (2015) argue that even a moderate breaking strain of  $\sim 0.065$  and a fracture extending to the base of the crust can power the most energetic giant flare to date.

Due to the large hydrostatic pressure in the NS crust  $P_{\text{crust}}$  in comparison to the shear modulus  $\mu$ , i.e.  $P_{\text{crust}} \gg \mu$ , it is impossible to create a long-lived void necessary for a brittle fracture to occur (Jones 2003), regardless of the magnitude of the imparted Maxwell stress. When the crust yields it does not crack, yet rather undergoes a gradual plastic deformation in response to the imparted Lorentz forces, whereby internal currents and associated magnetic helicity are transported outward into the less conductive magnetosphere (Thompson et al. 2002).

Levin & Lyutikov (2012) argue that the presence of a strong magnetic field reinforces the crust, which might strongly impede the formation of a propagating fracture or

<sup>2</sup> See also the discussion in Link (2014) on the feasibility of such an internal MHD instability mechanism.

<sup>3</sup> This mechanism was discussed earlier by Thompson & Duncan (1995) in explaining the physical process behind the less energetic recurrent soft  $\gamma$ -ray bursts from magnetars.

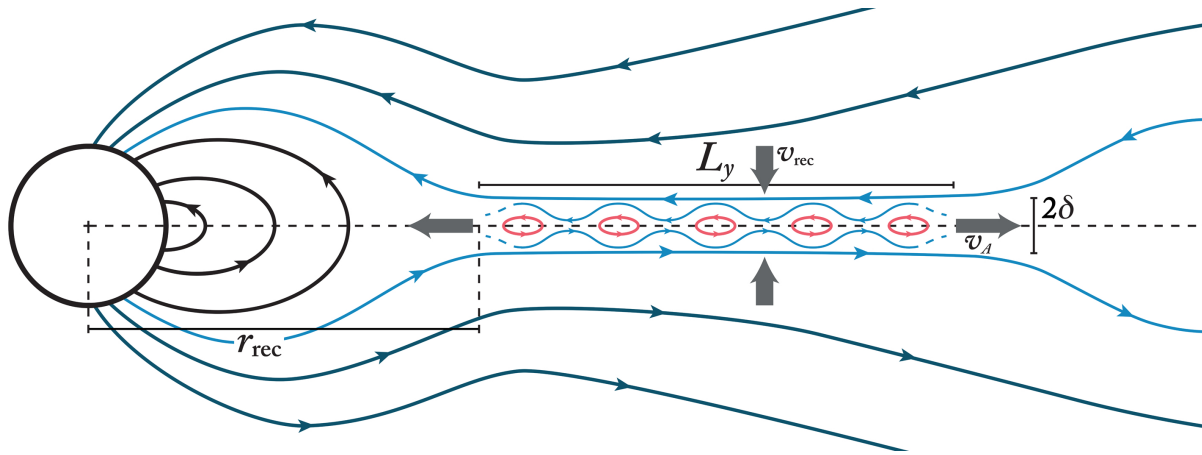


**Figure 1.** 2D cut-through of the globally sheared magnetic field containing an equatorial current sheet. Continuous current injections into the magnetosphere gradually increase the magnetic helicity of the external field. This in turn may evolve continuously towards a Y-type neutral line configuration, such that a narrow current sheet is formed. Reconnection through spontaneous tearing of the current sheet results in magnetic field dissipation and the ejection of a relativistic magnetic plasmoid. The dimensions of the current sheet have been labeled (current sheet length  $L_y$  and thickness  $2\delta$ ) and the height of the base of the reconnection region with respect to the centre of the NS is given by  $r_{\text{rec}}$ . The velocities  $v_{\text{rec}}$  and  $v_A$  are the inward reconnection and outward (Alfvénic) bulk plasma velocity, respectively.

global slip, altogether. Only under certain specific conditions, where the magnetic flux surface is oriented almost perfectly perpendicular to the direction of shear (within  $10^{-3}$  radian), can enough energy be released through a propagating fracture to explain the observed emission.

An important challenge for trigger mechanisms that manifest internally, either a core MHD instability or crustal failure, is the significant impedance mismatch between the internal and external Alfvén velocities (Link 2014). As a result, magnetic energy that dissipates through shear waves cannot be transmitted to the magnetosphere fast enough to explain the (sub)millisecond rise of the initial transient phase of the giant flare. Instead, shear waves get reflected numerous times prior to leaving the stellar interior, extending the outward transmission time considerably.

### 1.1.3 External trigger

The aforementioned issues with internal triggers have led to the notion that prior to a giant flare the magnetic energy might be stored in the magnetosphere, rather than in the interior of the NS. Thompson et al. (2002) argue that the tightly wound internal magnetic field induces a strong current that in turn closes through a thin surface layer. This local surface layer will experience a Lorentz force, which causes the crust to rotate plastically. Anchored magnetic field lines are dragged along with the gyrating motion and a twist is gradually imparted to the external magnetic field. The twist supporting currents can be composed by charges stripped from the NS surface or – more likely – by pair creation in the magnetosphere (Beloborodov & Thompson 2007). Subsequently, the non-potential external field reacts to the new boundary conditions and evolves through a series of quasi-equilibria, continuously twisting the external field either locally (Huang & Yu 2014a,b; Beloborodov 2009) or globally (Thompson et al. 2002).

A local increase of helicity leads to the formation of a helically twisted flux rope embedded in the magnetar mag-

netosphere, whereby the impulsive phase of the giant flare is associated with an abrupt loss of equilibrium and subsequent catastrophic destabilisation of the flux rope, analogous to the dynamics of coronal mass ejections (CMEs) (Masada et al. 2010; Yu 2012, 2013; Huang & Yu 2014a,b). Alternatively, a global accumulation of twist may cause the external field to eventually expand outwards, becoming increasingly radial, and admitting a cusp-shaped or Y-type neutral line topology, characterised by a narrow equatorial current sheet where the magnetic shear is most significant (Mikić & Linker 1994; Wolfson 1995; Parfrey et al. 2013). In this narrow yet extended neutral layer the gradients become significant and the MHD approximation breaks down allowing for the field lines to diffuse through the plasma. The onset of the flare is then given by an explosive reconnection event, which may roughly develop on the external Alfvén crossing time  $\tau_A^{\text{ext}} \sim 10^{-2}$  ms [Eq. (2)] (Thompson & Duncan 1995), and the expulsion of a relativistic plasmoid. In this paper we investigate specifically the reconnection process in the latter configuration – illustrated in Figure 1.

Both magnetospheric models provide a mechanism for slow build up of an energy reservoir over tens of years caused by the ambipolar diffusion of the internal magnetic field and its subsequent rapid conversion into bulk kinetic energy, particle acceleration, and radiation ( $\lesssim$  milliseconds). Observed spectral hardening (softening) and an increase (decrease) in spin down in the pre (post) giant flare stage of SGR 1900+14 and SGR 1806-22 (Woods et al. 1999, 2001; Mereghetti et al. 2005; Rea et al. 2005) are consistent with an increase (decrease) of twist and charge density in the external field (Thompson et al. 2002; Lyutikov 2006). Moreover, a considerable reduction in harmonic content of the pulse profile of SGR 1900+14 during and following the giant flare suggests a burst mechanism which reduced the twist of the external field significantly (Woods et al. 2001).

Distinct reconnection models have been introduced to describe the initial transient phase of the observed giant flares. Lyutikov (2003, 2006) and Komissarov et al. (2007)

suggest the development of the tearing instability in a relativistic force-free current sheet as the trigger mechanism. They argue that the minimum growth time of the linear tearing mode accords with the (sub)millisecond rise (to peak) of the giant flares. Alternatively, Gill & Heyl (2010) propose a fast reconnection model that relies on collisionless Hall reconnection ( $\tau_{\text{rec}}^{\text{Hall}} \sim 0.3$  ms) and ascribes a crucial role to the soft precursors ( $\gtrsim 10^{41}$  erg,  $k_{\text{B}}T < 50$  keV) that have been observed before the last two giant flares<sup>4</sup>. These precursors facilitate the conditions for collisionless Hall reconnection by introducing a baryon contaminant in the pair dominated magnetosphere, since the former process relies on the Hall effect which in turn requires a non-mass-symmetric plasma composition to operate.

In this article we focus on magnetospheric giant flare trigger mechanisms. In particular we critically analyse the most discussed candidate reconnection mechanism, i.e. impulsive reconnection through the spontaneous development of the tearing instability in a globally sheared external field.<sup>5</sup> We revise the tearing mode growth time as applied to magnetar magnetospheres by Lyutikov (2003) and expand on the rectified result. Characteristic timescales appearing in the giant flare lightcurves have hereby provided necessary constraints. Furthermore, we provide order of magnitude estimates related to the geometry of the reconnection region and discuss the validity of basic assumptions regarding this trigger mechanism.

In Section 2 we review typical timescales of the observed giant flare emission and additional relevant data of the phenomena involved. In Section 3 we summarise previous works on the dynamics behind the relativistic tearing instability and the general expression for its minimum growth time. Subsequently we show that a revised version of the tearing mode growth time for magnetar magnetospheres can in principle explain the (sub)millisecond rise times of giant flares under certain conditions, pertaining to the geometry of the reconnection region. In Section 4, using straightforward theoretical models that rely on the tearing mode timescale, we constrain the height of the reconnection region and thickness of the current sheet in which the tearing mode develops. In section 5 we discuss the relations between the MHD

<sup>4</sup> Any precursor of the 1979 March 5 giant flare would have gone by unnoticed due to the lack of detectors operational at the time with sensitivities below  $\sim 50$  keV.

<sup>5</sup> Recent particle-in-cell simulations that describe relativistic reconnection in pair plasmas demonstrate the growth of the drift-kink (DK) instability perpendicular to the plane of reconnection through tearing (Zenitani & Hoshino 2007). For certain initial equilibrium configurations the DK instability dominates over the tearing instability at first and consequently impedes efficient reconnection, thermalises the particles, and broadens the current sheet. However, it is also shown that efficient reconnection leading to significant particle acceleration will occur at a later stage, when the tearing mode regains dominance (Sironi & Spitkovsky 2014). Moreover, it is found that the DK instability is quenched in the presence of a finite guide field, such that the dynamics of the sheet is dictated by the development of the tearing instability at all stages (Zenitani & Hoshino 2008; Kagan et al. 2013; Cerutti et al. 2014). The  $B_{\phi}$  component of the globally twisted magnetic field surrounding the neutron star may act as a guide field in the case of an equatorial current sheet.

growth time and the radiative timescale, which is directly connected with the observed lightcurve. Throughout the article we adopt a Gaussian-cgs unit system in our calculations.

## 2 EMISSION TIMESCALES

Currently, three magnetars have produced a giant  $\gamma$ -ray flare. In chronological order they are the 1979 March 5 flare from SGR 0526-66 (Mazets et al. 1979), the 1998 August 27 flare from SGR 1900+14 (Hurley et al. 1999), and the 2004 December 27 flare from SGR 1806-20 (Palmer et al. 2005). The energy in radiation emitted during the decaying tail was roughly equal for the three giant flares ( $E_{\text{tail}} \sim 10^{44}$  erg), indicating that the strength of the confining magnetospheric field, which traps the photon-pair fireball, is roughly similar for the three sources since the energy storage capacity of the field is related to its strength (Mereghetti 2008). The inferred surface dipole magnetic field strengths  $B_s$  of the sources are given in Table 1. The released photon energy during the initial spike was however considerably larger for the most recent giant flare ( $E_{\text{spike}} \sim 10^{46}$  erg), as compared to the first two ( $E_{\text{spike}} \sim 10^{44}$  erg).

Considering the fact that the duration of the hard spike is roughly three orders of magnitude less than the soft tail, it is rather astonishing that the photon energy output of the hard spike is approximately equal to or even much greater than the energy released during the decay of the soft tail. The conversion of such a vast amount of stored magnetic energy into high energy radiation in a considerably limited window of time, requires an extraordinary trigger mechanism indeed, which accordingly may be constrained by the observed photon flux and associated sub(milli)second rise time.

### 2.1 Timescale definitions

In studying the initial spectrally hard phase of the giant flare lightcurve, the following characteristic emission timescales may be defined<sup>6</sup> (see Figure 2). The  $e$ -folding rise time  $\tau_e$  describes the exponential rise of the spike out from the continuum ( $[f_{\gamma} \propto \exp(t/\tau_e)]$ , where  $f_{\gamma}$  represents the photon flux). This emission timescale constrains the explosive capability of the trigger mechanism, i.e. the physical process that generates the observed radiation is necessarily required to advance on this timescale. The peak time  $\tau_{\text{peak}} \equiv |t_{\text{peak}} - t_0|$  denotes the time between the onset of the spike  $t_0$  and the moment  $t_{\text{peak}}$  when the spike photon flux peaks [ $f_{\gamma}^{\text{max}}(t_{\text{peak}})$ ] and the spike time  $\tau_{\text{spike}} \equiv |t_* - t_0|$  represents the duration of the spike, i.e. the timespan of the spectrally hard phase of the giant flare lightcurve, where  $t_*$  indicates the end time of the hard spike. The latter timescale may serve to constrain the energy deposition or radiative evaporation time. This timescale will depend on factors such as the extent of the energy reservoir, the rate of energy conversion and radiation production, and/or the effective trapping of the generated radiation.

<sup>6</sup> Here we follow the definitions for the typical timescales as described by Duncan (2004), section 1.3.

**Table 1.** Observed emission timescales from magnetar giant flares. Including auxiliary parameters: source distance  $d$ , isotropic peak luminosity  $L_{\text{peak}}$ , spike energy  $E_{\text{spike}}$ , spectral temperature  $k_{\text{B}}T_{\text{spec}}$ , and inferred surface dipole magnetic field strength  $B_{\text{s}}$ .

SGR		0526-66		1900+14		1806-20	
Date		1979 March 5		1998 August 27		2004 December 27	
			<i>Ref.</i>		<i>Ref.</i>		<i>Ref.</i>
$\tau_e$	[ms]	$\lesssim 1$	[4]	$< 1.6, < 4$	[14], [6]	$\lesssim 0.3, < 1$	[13], [7]
$\tau_{\text{peak}}$	[ms]	$\sim 15, \sim 20$	[8], [2]	-		$\sim 1.5$	[13]
$\tau_{\text{spike}}$	[s]	$\sim 0.1 - 0.2$	[9]	$\sim 0.35, \sim 1.0$	[10], [6]	$\sim 0.2, \sim 0.5$	[7], [13]
$d$	[kpc]	53.6	[5] <sup>†</sup>	12.5	[3] <sup>†</sup>	8.7	[1] <sup>†</sup>
$L_{\text{peak}}^*$	$[10^{44} \text{ erg s}^{-1}]$	$\sim 4.7, \sim 18^{**}$	[8], [4]	$> 0.64, > 5.6, > 160$	[6], [10], [14]	$\sim 7 \times 10^2$	[7]
$E_{\text{spike}}^*$	$[10^{44} \text{ erg}]$	$\sim 1.1$	[8]	$> 0.10, > 3.0$	[10], [14]	$\sim 1.2 \times 10^2$	[7]
$k_{\text{B}}T_{\text{spec}}$	[keV]	246	[4]	240	[6]	175	[7]
$B_{\text{s}}$	$[10^{14} \text{ G}]$	5.6	[15] <sup>†</sup>	7.0	[11] <sup>†</sup>	20	[12] <sup>†</sup>

\*Reference peak luminosities and spike energies have been adjusted according to respective source distances in [5], [3], and [1]. \*\*Peak luminosity from [8] ([4]) is an average over 200 (10) ms. *References:* [1] Bibby et al. (2008); [2] Cline et al. (1980); [3] Davies et al. (2009); [4] Fenimore et al. (1996); [5] Haschke et al. (2012); [6] Hurley et al. (1999); [7] Hurley et al. (2005); [8] Mazets et al. (1979); [9] Mazets & Golenetskii (1981); [10] Mazets et al. (1999); [11] Mereghetti et al. (2006); [12] Nakagawa et al. (2009); [13] Palmer et al. (2005); [14] Tanaka et al. (2007); [15] Tiengo et al. (2009). <sup>†</sup>References obtained through the ‘McGill Online Magnetar Catalog’ (Olausen & Kaspi 2014): <http://www.physics.mcgill.ca/~pulsar/magnetar/main.html>. Burst references can also be found at the Amsterdam Magnetar Burst Catalogue: <http://staff.fnwi.uva.nl/a.l.watts/magnetar/mb.html>.

## 2.2 Observed characteristic timescales and auxiliary parameters

From the giant flare initial spike data listed in Table 1, we find that the values for the various timescales are typically,  $\tau_e \sim 0.1 - 1$  ms,  $\tau_{\text{peak}} \sim 1 - 10$  ms, and  $\tau_{\text{spike}} \sim 0.1 - 1$  s. However, the accuracy and precision of the  $e$ -folding rise time measurements is restricted by the limited time-resolution of the detectors operational at the time. Moreover, the short timescales may have been significantly affected by saturation of the detector and deadtime of the instrument. Both effects, if present, result in an overestimation of the shortest timescales and in particular the  $e$ -folding rise times. Therefore strictly one should regard these timescales as upper limits.

The listed spectral temperatures  $k_{\text{B}}T_{\text{spec}}$  in Table 1 are obtained through fitting optically thin thermal Bremsstrahlung (OTTB) or cooling blackbody models to the spectra of the observed giant flare spikes (Fenimore et al. 1996; Hurley et al. 1999, 2005). However, the exact physical mechanism that generates the observed spectra remains unknown.

The initial spikes display strong variability on (sub)millisecond timescales and quasi-periodic oscillations (QPOs) with  $\nu \sim 10^2$  Hz (Barat et al. 1983; Hurley et al. 1999; Feroci et al. 2001; Terasawa et al. 2005; Schwartz et al. 2005). Peak luminosities and spike energies in Table 1 are found assuming isotropic radiation and computed from the observed fluxes using the respective source distances; no spectral bolometric corrections have been applied. In Table 1, multiple values are quoted at times for various quantities. These values have been sourced from distinct references. They differ because of significant differences in instrumentation, e.g. energy bandwidth and time resolution, and in data analysis techniques. We quote these values to give an indication of the uncertainties involved.

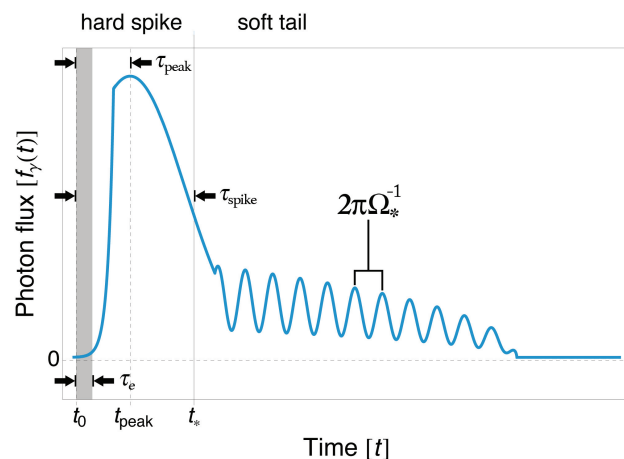


**Figure 2.** Schematic representation of giant  $\gamma$ -ray flare lightcurve with the  $\gamma$ -ray photon flux as a function of time. Typically the giant flare light curve may be subdivided into two regions characterised by their respective spectral hardness: the spectrally hard impulsive phase, i.e. the hard spike, and the spectrally soft afterglow or tail with superimposed pulsations. The onset of the giant flare is at  $t_0$ , the hard spike reaches its peak flux at  $t_{\text{peak}}$ , and  $t_*$  denotes the end of the spectrally hard phase. The grey area denotes the exponential rise timescale of the spike,  $f_{\gamma} \propto \exp(t/\tau_e)$ . The peak time is defined as  $\tau_{\text{peak}} \equiv |t_{\text{peak}} - t_0|$  and the spike duration time as  $\tau_{\text{spike}} \equiv |t_* - t_0|$ . Note that, since in reality  $\tau_{\text{spike}} \ll \tau_{\text{tail}}$ , the time domain of the initial phase has been magnified for viewing purposes. The most distinct mode of the modulated tail emission has a period equal to the rotation period  $2\pi\Omega_*^{-1}$  of the NS.

## 3 THE RELATIVISTIC TEARING MODE

Here we consider the development of the tearing instability in a relativistic current sheet as depicted in Figure 1. In the presence of finite magnetic resistivity  $\eta$  the current sheet will

become unstable to transverse tearing modes ( $\mathbf{k} \cdot \mathbf{B} = 0$ ) and decompose into many smaller current filaments or magnetic islands (Furth et al. 1963) – see Figure 1. Simultaneously magnetic energy is converted into heat, bulk kinetic energy, and charged particles are accelerated by the induced reconnection electric field  $\mathbf{E} = -E_z \hat{\mathbf{z}}$  (see e.g. Priest & Forbes 2000).

In the following we revisit and further analyse the (relativistic) tearing instability as a candidate trigger mechanism for the onset of magnetar giant flares, the groundwork for which has been laid in detail by Lyutikov (2003) and Komissarov et al. (2007). Here we briefly review the relevant equations of resistive magnetodynamics and the stability analysis of a current sheet in a magnetically dominated magnetosphere, which ultimately results in a minimum growth time of the linear tearing mode. Next we discuss the application of this characteristic timescale to the initial rise of magnetar giant flares and reassess the conclusions of previous work.

### 3.1 Force-free degenerate electrostatics

#### 3.1.1 Magnetization parameter

To investigate the properties of the magnetar magnetosphere it proves useful to define the dimensionless magnetization parameter,

$$\sigma_m \equiv 2 \frac{u_B}{u_p} = \frac{B^2}{4\pi\rho c^2}, \quad (4)$$

which describes the ratio of magnetic energy density to total particle energy density, where  $u_B = B^2/8\pi$  and  $u_p = \rho c^2$ , with  $B$  the magnitude of the magnetic field,  $\rho$  the particle density, and  $c$  the speed of light. The magnetization parameter for magnetar magnetospheres is estimated to be  $10^{13} \leq \sigma_m \leq 10^{16}$  (Komissarov et al. 2007). When  $\sigma_m \gg 1$ , the magnetosphere is said to be magnetically dominated (the inertia of the particles is negligible, even though they still act as carriers of charge) and relativistic, since the velocity of an Alfvén wave,

$$v_A = c \left( \frac{\sigma_m}{1 + \sigma_m} \right)^{1/2}, \quad (5)$$

approaches the speed of light, i.e.  $v_A \rightarrow c$ . Note accordingly that the Alfvén transit time becomes the light crossing time,  $\tau_A \rightarrow \tau_c = l/c$ , where  $l$  denotes the typical length scale of the system.

In describing the dynamics of the magnetar magnetosphere,  $\sigma_m^{-1}$  may be used as a small expansion parameter to approximate the general equations of relativistic magnetohydrodynamics (RMHD) in the limit of vanishing rest-mass density and pressure of matter (force-free approximation), i.e. force-free degenerate electrostatics (FFDE) or ‘magnetodynamics’ (MD) (Uchida 1997; Komissarov 2002; Komissarov et al. 2007).

#### 3.1.2 Ohm’s law in resistive FFDE

In FFDE the energy-momentum equation in covariant form, stripped from its matter component, reduces to

$$\nabla_\mu T_{em}^{\mu\nu} = 0, \quad (6)$$

where

$$T_{em}^{\mu\nu} = \frac{1}{4\pi} \left[ F^{\nu\alpha} F^\mu{}_\alpha - \frac{1}{4} g^{\mu\nu} (F_{\alpha\beta} F^{\alpha\beta}) \right], \quad (7)$$

denotes the electromagnetic stress-energy tensor, composed of the electromagnetic field tensor  $F^{\mu\nu}$  and the metric tensor  $g^{\mu\nu}$ . We do not consider the effects of gravitational curvature and assume a Minkowski metric  $g^{\mu\nu} \rightarrow \eta^{\mu\nu}$  with signature  $s = -2$ . Combining the energy-momentum equation [Eq. (6)] with the covariant homogeneous and inhomogeneous Maxwell’s equations, respectively

$$\partial_\mu (\star F)^{\nu\mu} = 0, \quad (8)$$

and

$$\partial_\mu F^{\mu\nu} = \frac{4\pi}{c} J^\nu, \quad (9)$$

where  $(\star F)^{\mu\nu} = (1/2)\epsilon^{\mu\nu\sigma\lambda} F_{\sigma\lambda}$  represents the Hodge dual of  $F^{\mu\nu}$  and  $J^\mu = (c\rho_{ch}, \mathbf{j})^T$  is the four-current<sup>7</sup>, we may write the divergence of the stress-energy tensor as

$$\partial_\nu T_{em}^{\mu\nu} - \frac{1}{c} F^{\mu\nu} J_\nu = 0, \quad (10)$$

and subsequently find

$$F^{\mu\nu} J_\nu = 0. \quad (11)$$

The above expression is the so-called force-free condition and implies specifically that the Lorentz force,

$$f^\mu = \frac{1}{c} F^{\mu\nu} J_\nu \quad (12)$$

is required to vanish, i.e. that the force-free electromagnetic field is fundamentally degenerate (Komissarov 2002). It follows immediately that the first electromagnetic invariant is zero,

$$F_{\mu\nu} (\star F)^{\mu\nu} = 0, \quad (13)$$

which is known as the degeneracy condition. This means that the inertia of the plasma particles, but not their electromagnetic interaction, is ignored.

In ideal FFDE we wish to describe the plasma velocity in a physical force-free electromagnetic field. To this end we require the plasma velocity field given by  $U^\mu = \gamma(c, \mathbf{v})^T$  to satisfy  $F_{\mu\nu} U^\nu = 0$ . Since the four-velocity of the plasma is a time-like vector, we demand that the second electromagnetic invariant is positive,

$$F_{\mu\nu} F^{\mu\nu} > 0, \quad (14)$$

which necessitates the existence of time-like zero eigenvectors of  $F_{\mu\nu}$ . This condition implies that there exists a reference frame wherein observers at rest detect a field that is purely magnetic, i.e. where the electric field vanishes entirely (Uchida 1997).

Adopting 3+1-notation we find that Eq. (11), Eq. (13), and Eq. (14) become respectively

$$\rho_{ch} \mathbf{E} + \frac{1}{c} \mathbf{j} \times \mathbf{B} = 0, \quad (15)$$

$$\mathbf{E} \cdot \mathbf{B} = 0, \quad (16)$$

$$B^2 - E^2 > 0, \quad (17)$$

<sup>7</sup> Here  $\rho_{ch}$  represents the plasma charge density.

where  $E$  denotes the magnitude of the electric field and  $B$  the magnitude of the magnetic field. Incidentally,  $F^{0i}J_i = \mathbf{E} \cdot \mathbf{j} = 0$  and the electromagnetic energy is conserved, i.e.

$$\partial_t(\mathbf{E} \cdot \mathbf{B}) = 0. \quad (18)$$

To obtain Ohm's law, which describes the relation between the current and the electric field, it is convenient to separate the current vector into components parallel and perpendicular to the magnetic field vector,

$$\mathbf{j} = \mathbf{j}_\perp + \mathbf{j}_\parallel, \quad \mathbf{j}_\perp = \frac{(\mathbf{B} \times \mathbf{j}) \times \mathbf{B}}{B^2}, \quad \mathbf{j}_\parallel = \frac{(\mathbf{B} \cdot \mathbf{j}) \mathbf{B}}{B^2}. \quad (19)$$

With the force-free condition Eq. (15) we may express the perpendicular component as

$$\mathbf{j}_\perp = \rho_{\text{ch}} \mathbf{v}_\perp \quad (20)$$

where along with the requirement expressed by Eq. (17) we have defined the electric drift velocity

$$\mathbf{v}_\perp \equiv c \frac{\mathbf{E} \times \mathbf{B}}{B^2}, \quad (21)$$

which denotes the plasma velocity component across the magnetic field.

In the singular current sheet however the ideal MHD approximation breaks down and the magnetic resistivity becomes finite, i.e. the second electromagnetic invariant [Eq. (17)] becomes negative. Accordingly, the parallel component of Ohm's law is altered to include the effect of current dissipation, solely along the magnetic field, due to the presence of a resistive electric field. To this end we introduce the relativistic formulation of Ohm's law in covariant form (Gedalin 1996),

$$F^{\mu\nu} U_\nu = \frac{4\pi}{c} \Theta^{\mu\nu} (\delta_\nu^\alpha - U_\nu U^\alpha) J_\alpha, \quad (22)$$

where  $\Theta^{\mu\nu}$  represents the resistivity tensor. This tensor is highly anisotropic in FFDE, since only the currents flowing along the field may experience resistive dissipation. Accordingly we define the resistivity tensor as such

$$\Theta^{\mu\nu} \equiv \eta \frac{b^\mu b^\nu}{b^2}, \quad (23)$$

where  $b^\mu = (\star F)^{\mu\nu} U_\nu$  represents the magnetic four-vector and the scalar resistivity or magnetic diffusivity, which characterises the dissipation of currents, is given by the phenomenological parameter<sup>8</sup>  $\eta = c^2/(4\pi\sigma)$ , with  $\sigma$  the macroscopic conductivity of the plasma. Subsequently, by convolving Eq. (22) with the magnetic four-vector we obtain (Lyutikov 2003)

$$F^{\mu\nu} U_\nu (\star F)_{\mu\alpha} U^\alpha = \frac{4\pi}{c} \eta (\star F)_{\mu\alpha} U^\alpha J^\mu, \quad (24)$$

which in 3+1 notation becomes

$$\gamma^2 (\mathbf{B} \cdot \mathbf{E}) (c^2 - \mathbf{v} \cdot \mathbf{v}) = \frac{4\pi}{c} \eta \gamma [\mathbf{j} \cdot (c\mathbf{B} - \mathbf{v} \times \mathbf{E}) - J^0 (\mathbf{B} \cdot \mathbf{v})], \quad (25)$$

where  $\gamma = [1 - (\mathbf{v} \cdot \mathbf{v}/c^2)]^{-1/2}$  is the Lorentz factor. The above expression reduces to

$$\frac{c^2}{4\pi\eta} (\mathbf{B} \cdot \mathbf{E}) = \frac{\gamma}{c} [\mathbf{j} \cdot (c\mathbf{B} - \mathbf{v} \times \mathbf{E}) - J^0 (\mathbf{B} \cdot \mathbf{v})]. \quad (26)$$

<sup>8</sup> We do not derive  $\eta$  from microscopic plasma processes, but rather assume a simple macroscopic description.

Upon splitting vectors into components parallel and perpendicular to the magnetic field we can rewrite Eq. (26) as

$$\frac{c^2}{4\pi\eta} (\mathbf{B} \cdot \mathbf{E}) = \gamma \left[ (\mathbf{B} \cdot \mathbf{j}) \left( 1 - \frac{E_\perp^2}{B^2} \right) - \rho_{\text{ch}} (\mathbf{B} \cdot \mathbf{v}) \left( 1 - \frac{E_\perp^2}{B^2} \right) \right]. \quad (27)$$

We remove the second term on the r.h.s. by choosing our coordinate system such that  $v_\parallel \equiv 0$ . Consequently with Eq. (21) we have that,

$$\gamma^{-2} = \left( 1 - \frac{E_\perp^2}{B^2} \right), \quad (28)$$

such that Eq. (27) becomes

$$(\mathbf{B} \cdot \mathbf{j}) = \frac{c}{4\pi} \left[ \frac{c\gamma}{\eta} (\mathbf{B} \cdot \mathbf{E}) \right]. \quad (29)$$

Accordingly we use the above result to rewrite the parallel component of the current vector and ultimately obtain the following expression for the current vector,

$$\mathbf{j} = \frac{c}{4\pi} \left[ 4\pi\rho_{\text{ch}} \frac{\mathbf{v}_\perp}{c} + \frac{c\gamma}{\eta} \frac{(\mathbf{B} \cdot \mathbf{E}) \mathbf{B}}{B^2} \right], \quad (30)$$

which describes Ohm's law in resistive FFDE, whereby the electric current is written solely in terms of the electric field components, parallel and perpendicular to the magnetic field. Note that in the plasma rest frame  $\mathbf{v}_\perp = 0$ , the electromagnetic field is no longer purely magnetic, due to the presence of the resistive electric field.

### 3.2 Magnetodynamics near force-free equilibrium

The divergence of the stress-energy tensor Eq. (10) determines the energy- and momentum conservation equations, given in 3+1 notation as follows

$$\partial_t u_{\text{em}} + \nabla \cdot \mathbf{S} + \mathbf{E} \cdot \mathbf{j} = 0, \quad (31)$$

$$\partial_t \mathbf{p}_{\text{em}} - \nabla \cdot \mathbf{T}_{\text{em}}^{ij} + \frac{1}{c} \mathbf{j} \times \mathbf{B} + \rho_{\text{ch}} \mathbf{E} = 0, \quad (32)$$

where respectively

$$u_{\text{em}} = \frac{B^2 + E^2}{8\pi} \quad \text{and} \quad \mathbf{p}_{\text{em}} = \frac{\mathbf{S}}{c^2}, \quad (33)$$

are the electromagnetic energy- and electromagnetic momentum density. The above expressions are written in terms of the Poynting vector,

$$\mathbf{S} = \frac{c}{4\pi} \mathbf{E} \times \mathbf{B}, \quad (34)$$

and the Maxwell stress-tensor

$$\mathbf{T}_{\text{em}}^{ij} = \frac{1}{4\pi} \left[ E^i E^j + B^i B^j - \frac{1}{2} (E^2 + B^2) \delta^{ij} \right], \quad (35)$$

where  $\delta^{ij}$  is the Euclidean metric of flat space.

To study the dynamical properties of a system near force-free equilibrium, we introduce the relevant timescales via the relativistic Lundquist number,

$$S_l \equiv \frac{\tau_\eta}{\tau_A} = \frac{lc}{\eta}, \quad (36)$$

where  $\tau_\eta \equiv l^2/\eta$  is the resistive diffusion timescale,  $\tau_A \equiv l/v_A \rightarrow l/c$  denotes the hydromagnetic timescale or Alfvén

transit time (for  $\sigma_m \gg 1$ ), and  $l$  denotes the corresponding typical length scale of the system.

The evolution of the system can be represented by the timescale  $\tau$ , for which  $\tau_A \ll \tau \ll \tau_\eta$ . Accordingly,  $|\mathbf{v}_\perp| \ll c$  and with Eq. (21) we find naturally  $E_\perp \ll B$ . Immediately we may approximate,

$$\begin{aligned} \gamma &\rightarrow 1, \\ u_{\text{em}} &\simeq u_B = \frac{B^2}{8\pi}, \\ \mathbf{T}_{\text{em}}^{ij} &\simeq \frac{1}{4\pi} \left( B^i B^j - \frac{B^2}{2} \delta^{ij} \right). \end{aligned}$$

Scaling Eq. (31) and Eq. (32) in terms of the small expansion parameters ( $\tau/\tau_\eta$ ) and ( $\tau_A/\tau$ ) and assuming incompressibility of the plasma, Komissarov et al. (2007) derive the following closed set of equations,

$$\nabla \cdot \mathbf{v}_\perp = 0, \quad (37)$$

$$\nabla \cdot \mathbf{B} = 0, \quad (38)$$

$$\partial_t \mathbf{B} = \nabla \times (\mathbf{v}_\perp \times \mathbf{B}) + \eta \nabla^2 \mathbf{B}, \quad (39)$$

$$\rho_{\text{em}}[\partial_t (\nabla \times \mathbf{v}_\perp)] = \frac{1}{8\pi} \nabla \times (\mathbf{B} \cdot \nabla) \mathbf{B}, \quad (40)$$

that together govern the dynamics of a system near force-free equilibrium and incidentally closely resemble the equations of non-relativistic resistive incompressible MHD.

### 3.3 Growth time of the (relativistic) tearing mode

#### 3.3.1 Linear stability analysis

The growth time of the tearing instability may be obtained by performing linear stability analysis on a current sheet described by the following one-dimensional force-free equilibrium profile that represents a rotational discontinuity (Low 1973),

$$\mathbf{B}_0 = B_0 \tanh\left(\frac{x}{\delta}\right) \hat{\mathbf{y}} \pm B_0 \text{sech}\left(\frac{x}{\delta}\right) \hat{\mathbf{z}}, \quad (41)$$

where the magnetic null line is given by the sheared  $B_{0y}$ -component that goes to zero at  $x = 0$ , whilst the magnitude of the magnetic field vector  $|\mathbf{B}_0(x)|$  remains constant under rotation over  $\pi$  radian (see Figure 3). The vector rotates predominantly within the domain  $-\delta < x < \delta$ , such that the typical length scale of the system is given by  $l \rightarrow \delta$ , which denotes the (half-)thickness of the current sheet<sup>9</sup>.

Through linearising the dynamical equations of resistive MD<sup>10</sup> Komissarov et al. (2007) demonstrate how to derive the following expressions for the (maximum) wavelength and (minimum) growth time of the fastest growing linear mode,

$$\lambda^{\text{max}} = 2\pi \delta \mathcal{S}_\delta^{1/4}, \quad \tau_{\text{min}}^{\text{min}} = \tau_A \mathcal{S}_\delta^{1/2} = (\tau_A \tau_\eta)^{1/2}, \quad (42)$$

where  $\mathcal{S}_\delta = c\delta/\eta$  is the relativistic Lundquist number corresponding to the length scale  $\delta$  and the minimum growth time

<sup>9</sup> In the following we refer to  $\delta$  simply as the thickness of the current sheet, even though in principle it only describes half of the total thickness - see Figure 1.

<sup>10</sup> The linearised equations of resistive MD are equal to those of resistive MHD, such that the growth time of the linear tearing mode remains equal for both regimes. This similarity was first made explicit by Komissarov et al. (2007).

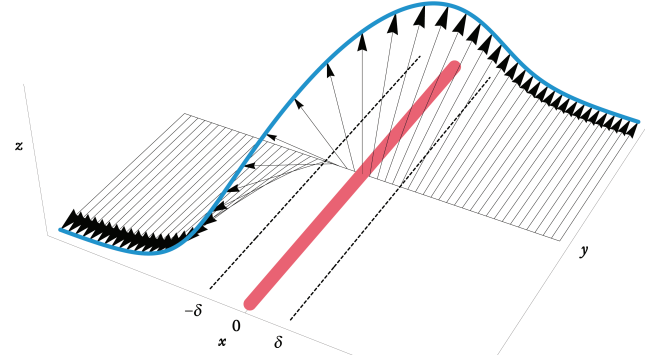


**Figure 3.** 3D schematic representation of the force-free equilibrium profile in the form of a rotational discontinuity. The magnitude of the magnetic field vector remains constant under rotation over  $\pi$  radian and most of the rotation takes place within  $-\delta < x < \delta$ . Accordingly, the typical length scale of the system, i.e. the current sheet (half-)thickness, is given by  $\delta$ . A magnetic null line, which denotes the location of the resistive sublayer, is formed in the  $xy$ -plane at  $x = 0$ .

of the tearing mode is ascertained to be the geometric mean of the Alfvén- and resistive diffusion timescale, as in the case of non-relativistic resistive incompressible MHD. Further comprehensive and general derivations of tearing mode characteristics may be found in the literature, e.g. White (1986), Goldston & Rutherford (1995), Priest & Forbes (2000), Lyutikov (2003), and Goedbloed et al. (2009).

### 3.4 Tearing mode growth time in magnetar magnetospheres

Here we aim to establish the minimum growth time of the tearing mode prevailing in magnetar magnetospheres. In a globally twisted magnetic field the radial dependency of the magnetic field strength is approximately given by (Thompson et al. 2002)

$$B_0(r) \simeq B_s \left( \frac{r}{R_*} \right)^{-(2+p)}, \quad (43)$$

where  $B_s$  denotes the inferred surface dipole magnetic field strength and  $R_* \sim 10^6$  cm is the typical NS radius. Also,  $0 < p < 1$  is the radial index which parameterises the net twist angle  $0 < \Delta\phi < \pi$ , where the limiting value  $p = 1$  ( $p = 0$ ) corresponds to a net twist of  $\Delta\phi = 0$  ( $\Delta\phi = \pi$ ), representing a pure dipole (split monopole) configuration.  $B_0(r)$  will function as the background or upstream magnetic field strength of the reconnection region.

We need a qualitative estimate of the local magnetic resistivity  $\eta$ . We consider a macroscopic description, whereby the resistivity is homogeneous and given by the presence of Langmuir turbulence (as in Lyutikov 2003). In this case the typical turbulent length scale is given by the electron skin depth,

$$\delta_e = \frac{c}{\omega_{p,e}} \quad (44)$$

where  $\omega_{p,e} = (4\pi n_\pm e^2/m_e)^{1/2}$  is the electron plasma frequency, with  $n_\pm = n_+ + n_-$  the total number density of the charge carriers, i.e. the sum of positrons  $n_+$  and electrons

$n_-$ ,  $e$  is the elementary charge unit, and  $m_e$  the electron mass. Accordingly, the resultant resistivity of a turbulent plasma with a typical eddy size and turnover velocity of  $\delta_e$  and  $c$  respectively, is approximately

$$\eta \sim c \delta_e = \frac{c^2}{\omega_{p,e}} = c^2 \left( \frac{4\pi n_{\pm} e^2}{m_e} \right)^{-1/2}. \quad (45)$$

In the aforementioned globally twisted dipole model the magnetospheric currents generate a toroidal field component that approaches the strength of the poloidal field, i.e.  $B_t \lesssim B_p \sim B_0(r)$ . Therefore we may apply Ampère's law to obtain an estimate for the charge number density as a function of the local magnetic field strength  $B_0(r)$  and distance from the NS centre  $r$  (Lyutikov 2002),

$$\nabla \times \mathbf{B}_0 = \frac{4\pi}{c} \mathbf{j} = 4\pi e [\beta_+ n_+ - \beta_- n_-], \quad (46)$$

where  $\beta_+$  and  $\beta_-$  are the dimensionless drift velocities of the positrons and electrons, respectively. If we consider the case where  $\beta_+ = -\beta_- \sim 1$  and  $n_+ \simeq n_-$ , we may simplify<sup>11</sup>

$$n_{\pm} \sim \frac{B_0(r)}{8\pi e r}. \quad (47)$$

Accordingly, we obtain an expression for the plasma frequency,

$$\omega_{p,e} \sim \left( \frac{\omega_{c,e} c}{r} \right)^{1/2}, \quad (48)$$

with the electron cyclotron frequency given by  $\omega_{c,e} \equiv eB_0(r)/(m_e c)$ . The resistivity as a function of the surface dipole magnetic field strength and distance to the centre of the NS becomes

$$\eta \simeq c^2 \left[ \frac{eB_s}{m_e r} \left( \frac{r}{R_*} \right)^{-(2+p)} \right]^{-1/2}. \quad (49)$$

Now together with Eq. (42) and Eq. (36) we may ultimately obtain the minimum growth time of the tearing mode in magnetar magnetospheres,

$$\tau_{\text{tm}}^{\text{min}} = \left( \frac{\delta^3}{c\eta} \right)^{1/2} \simeq \left( \frac{eR_*^{(2+p)}}{m_e c^6} \right)^{1/4} \delta^{3/2} r^{-(3+p)/4} B_s^{1/4}. \quad (50)$$

In order to compare this result with the observed timescales, we rewrite the above result in terms of typical values for the relevant parameters,

$$\tau_{\text{tm}}^{\text{min}} \simeq 10^{-1} \delta_4^{3/2} r_7^{-(3+p)/4} B_{s,15}^{1/4} \text{ ms}, \quad (51)$$

where we define  $\delta_4 \equiv \delta/(10^4 \text{ cm})$ ,  $r_7 \equiv r/(10^7 \text{ cm})$ ,  $B_{s,15} \equiv B_s/(10^{15} \text{ G})$ , and  $0 < p < 1$  (in practice  $p$  will always be close to unity). With these scalings, the minimum growth time of the tearing mode agrees nicely with the observed (sub)millisecond  $e$ -folding rise times  $\tau_e$  of the magnetar giant flares.

Note that this timescale differs significantly from the

minimum growth time as calculated by Lyutikov (2003), essentially due to an error in that calculation (specifically in the inferred expression for the plasma frequency). In addition we have adopted a rather smaller (by a factor of  $10^{-2}$ ) typical size for the thickness of the current sheet  $\delta$  than the value used in Lyutikov (2003). We do this since for large gradients to develop, the thickness of the current sheet must be significantly less than the global extent of the reconnection region, which in the case of magnetar giant flares is a few times the NS radius. Komissarov et al. (2007) argue for a current sheet thickness of  $\sim 3 \times 10^3 \text{ cm}$ , however we have not been able to reproduce their inferred tearing mode timescale (particularly Eq. (73) in their paper). Without the above modification to the typical value for  $\delta$ , however, the inferred tearing mode growth time would be  $\sim 100 \text{ ms}$  (Duncan 2004). If this were the case, it would entirely rule out the development of the tearing mode as a candidate mechanism to explain the (sub)millisecond rise times of the magnetar giant flares.

In the subsequent section we will assume that the trigger is given by the development of a tearing instability, and that its minimum growth time corresponds to the timescale on which the observed emission is released from the system, i.e.  $\tau_{\text{tm}}^{\text{min}} = \tau_e$ . We explore additional constraints on the geometry of the reconnection region that are required for the linear tearing mode to be a plausible mechanism for the giant flares, and discuss how they relate to the constraints derived in this section.

#### 4 PHYSICAL CONSTRAINTS ON THE RECONNECTION REGION

Here we present two straightforward models, respectively based on energy conservation and mechanical equilibrium of the current sheet, that provide order of magnitude estimates for the thickness of the current sheet  $\delta$  and height of the base of the reconnection region in terms of the radial distance from the NS centre  $r$ .

In order to relate the thickness of the tearing unstable current sheet to the global length of the reconnection region  $L_y$ , we consider the following elementary instability condition: for an unstable mode to be able to develop in a current sheet, its growth time ( $\tau_{\text{tm}}^{\text{min}}$ ) is required to be less than the time it would take for the perturbation to exit the system ( $L_y/c$ ) (Shibata & Tanuma 2001). We obtain the requirement

$$\tau_{\text{tm}}^{\text{min}} < \frac{L_y}{c}. \quad (52)$$

Together with Eq. (50) we have the following upper limit to the thickness of the current sheet

$$\delta^{\text{max}} = \delta^{-1/2} L_y, \quad (53)$$

and equivalently

$$\delta^{\text{max}} = [c\eta(\tau_{\text{tm}}^{\text{min}})^2]^{1/3}. \quad (54)$$

##### 4.1 Conversion of magnetic energy

Figure 4 shows the geometry of the reconnection region in the  $xy$ -plane, whereby the curved (blue) arrows represent the sheared magnetic field that continues to annih-

<sup>11</sup> Twisted magnetospheres are believed to be threaded by pairs moving at mildly relativistic speeds and with low multiplicity, as required to explain magnetars quiescent emission at X-ray energies (see e.g. Turolla et al. 2015, and references therein).

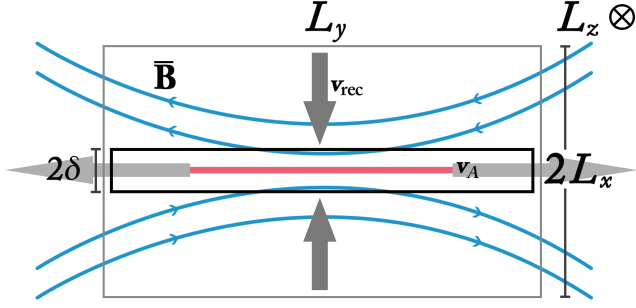


**Figure 4.** 2D schematic representation of the reconnection region – the reconnection geometry is uniform along the  $z$ -direction. The curved (blue) arrows denote the sheared magnetic field component, the thick arrows (grey) represent the plasma in- and outflows, the large box describes the extent of the reconnection region for the duration of the hard  $\gamma$ -ray spike, and the smaller rectangular box denotes the current sheet. The volume of the entire reconnection region is given by  $V = (2L_x)L_yL_z$ , where  $L_x = v_{\text{rec}}\tau_{\text{spike}} = (\delta/\tau_{\text{rec}})\tau_{\text{spike}}$ , representing the extent to which the magnetic field is fed into the diffusion region for the duration of the spike, assuming  $v_{\text{rec}}$  remains constant, and  $L_z < 2\pi r$  for an equatorial current sheet. This image essentially represents a magnification of the reconnection region depicted in Figure 1.

late within the current sheet, which in turn is denoted by the smaller rectangular box ( $2\delta \times L_y$ ). The larger rectangle ( $2L_x \times L_y$ ) describes the size of the total area that proceeds to reconnect, i.e. the extent of magnetic flux that is advected into the current sheet for the duration of the hard  $\gamma$ -ray spike  $\tau_{\text{spike}}$ . We hypothesise that the magnetic field lines are fed into the diffusion region at a constant rate (this assumption is discussed further in section 5.2.2). The reconnection rate is generally determined by the aspect ratio of the reconnection region through mass flux conservation (e.g. Pucci & Velli 2013), i.e.

$$\frac{v_{\text{rec}}}{c} \simeq \frac{\delta}{L_y} = S_{\delta}^{-1/2}, \quad (55)$$

which together with Eq. (52) leads to

$$v_{\text{rec}} \simeq \frac{\delta}{\tau_{\text{rec}}}. \quad (56)$$

Accordingly, we find that

$$L_x \sim v_{\text{rec}}\tau_{\text{spike}} = \delta \left( \frac{\tau_{\text{spike}}}{\tau_{\text{rec}}} \right). \quad (57)$$

For an equatorial current sheet we have  $L_z < 2\pi r$  (one may picture the current sheet as a disk around the NS if  $L_z = 2\pi r$ ). The entire volume of magnetic flux that reconnects over the course of the initial hard phase of the giant flare is then given by  $V = (2L_x)L_yL_z$ . The energy contained in this region, that is subsequently released within  $\tau_{\text{spike}}$  can be estimated as

$$E_{\text{tot}} \simeq \zeta u_B V = \zeta \frac{B_0^2}{8\pi} (2L_x L_y L_z) = \frac{\zeta B_0^2 r L_y \delta}{2} \left( \frac{\tau_{\text{spike}}}{\tau_{\text{rec}}} \right), \quad (58)$$

where  $\zeta$  is the fraction of free magnetic energy that is dissipated and we have used  $u_B = B_0^2/(8\pi)$  for the local magnetic energy density in terms of the upstream magnetic field  $B_0$ .

Rewriting this equation we obtain

$$\delta(r) \sim \frac{2 E_{\text{tot}}}{\zeta B_0^2 r L_y} \left( \frac{\tau_{\text{rec}}}{\tau_{\text{spike}}} \right). \quad (59)$$

Note incidentally that the above general expression does not rely on any particular reconnection mechanism as yet. If we now consider linear tearing as the principal reconnection mechanism, we may set  $\tau_{\text{rec}} = \tau_{\text{tm}}^{\text{min}}$  and, through Eq. (52),  $L_y = c\tau_{\text{tm}}^{\text{min}}$ . Using Eq. (43) and adopting  $p = 1/2$  we end up with

$$\delta(r) \sim \frac{2 E_{\text{tot}} r^4}{\zeta c B_s^2 R_*^5 \tau_{\text{spike}}}. \quad (60)$$

Together with the condition stated in Eq. (54), we find an estimate for the height of the reconnection region

$$r_{\text{rec}} \sim 10^7 \left[ \zeta B_{s,15}^{11/6} (\tau_{\text{tm},-4}^{\text{min}})^{2/3} \left( \frac{\tau_{\text{spike},0.2}}{E_{\text{tot},45}} \right) \right]^{12/41} \text{ cm}, \quad (61)$$

and the thickness of the current sheet at  $r_{\text{rec}}$ ,

$$\delta(r_{\text{rec}}) \sim 10^4 \left[ \zeta^7 B_{s,15}^6 (\tau_{\text{tm},-4}^{\text{min}})^{32} \left( \frac{\tau_{\text{spike},0.2}}{E_{\text{tot},45}} \right)^7 \right]^{1/41} \text{ cm}. \quad (62)$$

In the above we have made use of Eq. (49) and Eq. (52) to eliminate  $\eta(r)$  and  $L_y$  respectively. The solutions depend mildly on  $\zeta$ .

## 4.2 Mechanical equilibrium

Without mechanical equilibrium across the current sheet boundary, the current sheet would disrupt before reconnection could occur effectively (Uzdensky 2011). This requirement is given by the following pressure balance,

$$P_{\text{cs}} + \frac{B_{\text{cs}}^2}{8\pi} = P_0 + \frac{B_0^2}{8\pi}, \quad (63)$$

where  $P_{\text{cs}}$  and  $B_{\text{cs}}$  respectively are the leptophotonic pressure [see Eq. (65)] and magnetic field strength inside the current sheet, and  $P_0$  and  $B_0$  respectively are the local plasma pressure and magnetic field strength in the upstream region. In the upstream region we have  $\sigma_{\text{m}} \gg 1$ , such that the plasma beta,  $\beta = P_{\text{plasma}}/P_{\text{mag}}$ , is small, i.e.  $P_0 \ll B_0^2$ . Consequently, the above expression simplifies to

$$P_{\text{cs}} + \frac{B_{\text{cs}}^2}{8\pi} \simeq \frac{B_0^2}{8\pi}. \quad (64)$$

The leptophotonic pressure in the current sheet may be decomposed as

$$P_{\text{cs}} = P_{\text{rad}} + P_{\pm}, \quad (65)$$

where  $P_{\text{rad}}$  signifies the radiation pressure and  $P_{\pm}$  denotes the pressure as a result of pair production. In a relativistic current sheet  $P_{\pm}$  becomes  $\sim (7/4)P_{\text{rad}}$  (Uzdensky 2011), such that

$$P_{\text{cs}} \sim \frac{11}{4} P_{\text{rad}}, \quad (66)$$

and

$$P_{\text{rad}}(T_{\text{cs}}) = \frac{4 \sigma_{\text{SB}}}{3 c k_{\text{B}}^4} (k_{\text{B}} T_{\text{cs}})^4, \quad (67)$$

where  $\sigma_{\text{SB}} \equiv \pi^2 k_{\text{B}}^4 / (60 \hbar^3 c^2) \simeq 5.67 \times 10^{-5} \text{ erg cm}^{-2} \text{ s}^{-1} \text{ K}^{-4}$  is the Stefan-Boltzmann constant and  $T_{\text{cs}}$  represents the temperature inside the current sheet.

Eq. (64) may then be written as

$$B_0^2 - B_{\text{cs}}^2 = 22\pi P_{\text{rad}}. \quad (68)$$

Furthermore using Gauss's law for magnetism  $\nabla \cdot \mathbf{B} = 0$ , we approximate

$$\frac{B_{\text{cs}}}{\delta} + \frac{B_y}{L_y} + \frac{B_z}{L_z} \simeq 0, \quad (69)$$

where we respectively parameterise the strengths of the guide field and  $y$ -component of the field as  $B_g = qB_0$  and  $B_y = (1 - q)B_0$ , with  $0 \leq q \leq 1/2$  and  $\mathbf{B}_0 = \mathbf{B}_g + \mathbf{B}_y$ . Subsequently, we may write

$$B_{\text{cs}} \simeq B_0 \left[ (1 - q) \frac{\delta}{L_y} + q \frac{\delta}{L_z} \right]. \quad (70)$$

Together with Eq. (53) and the relation for  $L_z$  below Eq. (57) this becomes

$$B_{\text{cs}} \simeq B_0 \left[ (1 - q) \mathcal{S}_\delta^{-1/2} + q \frac{\delta}{2\pi r} \right], \quad (71)$$

such that we may eliminate  $B_{\text{cs}}$  from Eq. (68):

$$B_0^2 \left\{ 1 - \left[ (1 - q) \mathcal{S}_\delta^{-1/2} + q \frac{\delta}{2\pi r} \right]^2 \right\} = 22\pi P_{\text{rad}}. \quad (72)$$

The above equation depends on the values for  $B_s$ ,  $T_{\text{cs}}$ ,  $\delta$  and  $r$ . To solve Eq. (72) we need to write  $\delta$  in terms of  $r$  via Eq. (54) and require an estimate for the temperature *inside* the current sheet  $k_{\text{B}}T_{\text{cs}}$ . It is however questionable whether  $k_{\text{B}}T_{\text{spec}}$  – listed in Table 1 – would represent  $k_{\text{B}}T_{\text{cs}}$ , since the former may rather correspond to a Lorentz boosted photospheric temperature of a relativistically expanding fireball. Of necessity, we consider here the following reasonable range of temperatures:  $k_{\text{B}}T_{\text{cs}} \sim 250 - 1000 \text{ keV}$ .

Consequently, together with  $B_s = 10^{15} \text{ G}$  and  $\tau_{\text{tm}}^{\text{min}} = 10^{-4} \text{ s}$ , we solve Eq. (72) numerically for  $r$  and find,

$$r_{\text{rec}} \sim (3 \times 10^6) - 10^7 \text{ cm}, \quad (73)$$

and furthermore with Eq. (54) we have

$$\delta(r_{\text{rec}}) \sim (4 - 8) \times 10^3 \text{ cm}, \quad (74)$$

where the lower (upper) estimates of the above equations correspond to the upper (lower) value for  $k_{\text{B}}T_{\text{cs}}$ . These estimates remain equal down to the fourth decimal for the entire range of  $q$  and as one can observe from Eq. (71),  $B_{\text{cs}} \ll B_0$ , such that the second term on the l.h.s. of Eq. (68) may be neglected to find the following expression (for  $p = 1/2$ ),

$$r_{\text{rec}} \sim 10^7 B_{s,15}^{2/5} \left( \frac{k_{\text{B}}T_{\text{cs}}}{250 \text{ keV}} \right)^{-4/5} \text{ cm}. \quad (75)$$

Note that the results agree roughly with those obtained in the previous section. Additionally, we find that the dimensionless reconnection rate is approximately  $M_{\text{rec}} \equiv \delta / (v_A \tau_{\text{rec}}) \simeq \delta / (c \tau_{\text{tm}}^{\text{min}}) \sim 10^{-3}$ , which is comparable to the reconnection rates found for solar flares (e.g Narukage & Shibata 2006). Moreover, note that the reconnection region is located high up in the magnetosphere, such that the background magnetic field is sub-critical  $B_0(r_{\text{rec}}) \simeq 10^{12} \text{ G} \sim 10^{-1} B_{\text{qed}}$ .

## 5 DISCUSSION

### 5.1 Geometry of the reconnection region

The previous calculations provide estimates for the scale of the reconnection region involving spontaneous tearing of a global current sheet; the sheet length [from Eq. (52)] is  $L_y \gtrsim c \tau_{\text{tm}}^{\text{min}} = c \tau_e \sim (3 \times 10^6) - 10^7 \text{ cm}$ , the sheet thickness is  $\delta \sim 10^4 \text{ cm}$ , and the height of the reconnection region is  $r \sim 10^7 \text{ cm}$ . Here we briefly discuss various consequences of these results.

We have assumed that the resistivity is given by a homogeneous background of Langmuir turbulence, which fundamentally requires that the drift velocity of the current-carrying particles exceeds the thermal velocity of the background plasma. This needs to be the case throughout the extensive reconnection region ( $> 2\delta \times L_y$ ) for impulsive tearing to be able to occur on the requisite short timescales.

With an estimate for the thickness of the reconnection region, we can infer the temperature at the photosphere of the current sheet  $k_{\text{B}}T_{\text{phot}}$  (Uzdensky 2011). At the photosphere the optical depth

$$\tau \sim \frac{\delta}{\lambda_{\text{mfp}}}, \quad (76)$$

will be of order unity, where  $\lambda_{\text{mfp}}$  is the photon mean free path. Assuming that this temperature is sub-relativistic, such that the pair number density is given by

$$n_{\pm} = \frac{1}{\sqrt{2\pi^3}} \left( \frac{m_e c}{\hbar} \right)^3 \left( \frac{k_{\text{B}}T_{\text{phot}}}{m_e c^2} \right)^{3/2} \exp \left[ - \frac{m_e c^2}{k_{\text{B}}T_{\text{phot}}} \right], \quad (77)$$

and considering that the scattering opacity of O-mode (i.e. ordinary mode) photons in the presence of a strong magnetic field remains close to Thompson scattering opacity,  $\sigma_{\text{es}}(\text{O}) \sim \sigma_T \equiv (8\pi/3) e^4 / (m_e c^2)^2 \simeq 6.65 \times 10^{-25} \text{ cm}^2$ , we have

$$\lambda_{\text{mfp}}(\text{O}) \sim \frac{1}{n_{\pm} \sigma_T}. \quad (78)$$

Together with Eq. (76) we find

$$\delta \sigma_T n_{\pm}(k_{\text{B}}T_{\text{phot}}) \sim 1, \quad (79)$$

which can be solved for  $\delta \sim 10^4 \text{ cm}$  to get  $k_{\text{B}}T_{\text{phot}} \sim 27 \text{ keV}$ . Note however that  $k_{\text{B}}T_{\text{phot}}$  depends only weakly on  $\delta$ .

Due to the release of high-energy radiation following the reconnection process, extensive pair-production has resulted in a high photospheric pair density  $n_{\pm}(k_{\text{B}}T_{\text{phot}} \sim 27 \text{ keV}) \sim 10^{20} \text{ cm}^{-3}$ . Note that this pair density greatly exceeds the charge density that is available prior to the onset of reconnection [from Eq. (46) we establish  $n \gtrsim 10^{14} B_{s,15} r_7^{-7/2} \text{ cm}^{-3}$ ]. It is argued that the observed spectral temperatures  $k_{\text{B}}T_{\text{spec}}$  (see Table 1) correspond to a Lorentz-boosted photospheric temperature of a pair fireball that, in the wake of the onset of the flare, expands outward from the stationary reconnection region relativistically (Lyutikov 2006; Uzdensky 2011), such that

$$\Gamma k_{\text{B}}T_{\text{phot}} = k_{\text{B}}T_{\text{spec}}, \quad (80)$$

where  $\Gamma$  denotes the bulk Lorentz factor of the ejected fireball.<sup>12</sup> Using the result from Eq. (79) and assuming that the

<sup>12</sup> Note that the photosphere of the relativistically expanding fireball differs from the stationary emission region associated with

dimensions of the fireball roughly correspond to those of the initial current sheet, we obtain  $\Gamma \sim 10$ , which is consistent with previous estimates in literature.

Furthermore, considering the required scale of the initial configuration  $L_y$ , uniquely determined by  $\tau_e$ , spontaneous tearing seems an unlikely candidate for the smaller recurrent  $\gamma$ -ray bursts ( $\lesssim 10^{41}$  erg,  $\tau_e \sim 1$  ms (Göğüş et al. 2001; Gavril et al. 2004)), since their  $e$ -folding rise times are similar to those of the giant flares, such that  $L_y \sim (3 - 10)R_*$ . These particular bursts may rather demonstrate for instance driven reconnection through an external driver (e.g. sudden crustal motion at magnetic foot points or ideal instabilities in smaller critically sheared magnetic arcades (Browning et al. 2008)), or comprise explosive seismic events without involving magnetospheric reconnection altogether.

## 5.2 Linear tearing and the observed high energy emission

In discussing linear tearing as a candidate mechanism for explaining the fast initial rise of magnetar giant flare light curves, it has been implicitly assumed throughout the literature that the growth of the resistive instability directly coincides with the conversion of magnetic energy – via Ohmic heating and particle acceleration – into the observed high energy radiation (i.e.  $\tau_{\text{tm}}^{\text{min}} = \tau_e$ ) (Lytikov 2003; Duncan 2004; Komissarov et al. 2007). This conjecture presumes that (i) linear tearing dictates the rate of radiation release and (ii) that during the linear tearing phase a significant amount of magnetic energy is converted efficiently to produce the observed radiation in the first place. Both assumptions will be examined further; in Section 5.2.1 we discuss the former requisite (i), and in Sections 5.2.2 and 5.2.3 we address the latter (ii).

### 5.2.1 Nonthermal emission from accelerated particles

Concerning point (i) above it should be emphasised by observing that even for comparatively well-studied phenomena like solar flares the generation and release of radiation is not unequivocally linked to the reconnection rate. Note that whilst solar flares are not supposed to be directly analogous, the comparison may still be informative. The rapid onset of a solar flare is given by the sudden increase of hard X-ray (HXR) emission due to collisional thick-target Bremsstrahlung interactions of nonthermal particles at the chromospheric footpoints of coronal loop structures undergoing magnetic reconnection (Shibata & Magara 2011). Accordingly, the observed radiation timescales are determined by the acceleration timescales of the nonthermal particles.

Proposed acceleration mechanisms include direct acceleration by reconnection induced or field-aligned electric fields (e.g. Aschwanden 2006; Egedal et al. 2012), acceleration through shocks (Aschwanden 2006), and stochastic acceleration through turbulence excited by reconnection outflows at the loop top or cascading Alfvén waves near the footpoints (e.g. Petrosian & Liu 2004; Liu et al. 2008; Liu & Fletcher 2009; Fletcher & Hudson 2008). None of the above

the onset of the flare, such that the bulk Lorentz factor of the latter is zero.

processes guarantee a straightforward connection between the timescales of linear tearing and that of radiation release. Moreover, such acceleration mechanisms generally rely on the later phases of reconnection (e.g. nonlinear tearing; see section 5.2.3) or rather its large-scale effects, such as reconnection jets that excite MHD turbulence or the catastrophic rearrangement of the global magnetic field topology. In the latter case, the amount and rate of energy release will be determined more by the dynamic restructuring of the field, than on the dissipation of an extended current sheet (Hoshino & Lyubarsky 2012).

Efficient particle acceleration in magnetar magnetospheres may however require local regions where the magnetic field becomes small enough, since considerable synchrotron losses might otherwise impede any significant acceleration. Acceleration through reconnection induced electric fields localised at magnetic x-points seems fitting in this regard, since not only does  $B_y \rightarrow 0$  but the presence of  $\mathbf{E} \times \mathbf{B}$ -drift also focusses the trajectory of the charged particles in the acceleration region (Speiser 1965). Particle-in-cell (PIC) simulations of relativistic reconnection in pair plasmas disclose short acceleration timescales (Zenitani & Hoshino 2001), such that the timescale on which the radiation is generated is the reconnection rate.

Nonetheless, a major complication is given by the copious pair production that will ensue upon release of high energy radiation in the presence of an ultra-strong magnetic field (e.g. Harding & Lai 2006), causing the reconnection region to become optically thick. The observed radiation timescales will therefore not necessarily represent the timescales associated with reconnection dynamics (Uzdensky 2011; Hoshino & Lyubarsky 2012). To further constrain magnetar burst trigger mechanisms, via emission timescales, will require a better understanding of radiation transport in the magnetar magnetosphere.

### 5.2.2 Phases of tearing: linear and nonlinear

Exponential growth of the magnetic island proceeds until their half-width

$$w(t) \propto \exp\left[\frac{t}{\tau_{\text{tm}}}\right], \quad (81)$$

becomes comparable to the size of the resistive sublayer  $\epsilon\delta$ ; here nonlinear effects become important. Analytic calculations disclose a transition from exponential to algebraic growth ( $\propto t^\alpha$ ), once this stage is reached (Rutherford 1973). Numerical simulations confirm this strong change in reconnection rate, even though it is less significant when  $k \ll 1$  and  $S_\delta \gg 1$  (Steinolfson & van Hoven 1984). Moreover, it is found that the nonlinear regime sets in very quickly, after only a few  $e$ -folding times, such that one would expect to observe a considerable change in reconnection rate just moments after the onset of the instability. With  $\tau_{\text{tm}}^{\text{min}} \sim 10^{-4}$  ms, the exponential phase of the light curve would only last a few tenths of milliseconds to a millisecond, followed by a notable decline in count rate due to the transition from linear to nonlinear tearing. A break in the increase of the count rate during the initial rise to peak has been observed for the SGR 1806-20 flare by Terasawa et al. (2005), Schwartz et al. (2005), and Tanaka et al. (2007) after a few  $e$ -folding times.

The latter reference also finds a similar break in the SGR 1900+14 giant flare.

Note that the assumption of a constant reconnection rate for the duration of the hard spike ( $\tau_{\text{spike}} \sim 0.1 - 1$  s), as applied in Section 4.1, is suspect in the light of nonlinearity of the mode; the obtained estimates for  $r$  and  $\delta$  [Eq. (61) and Eq. (62)] are lower limits in this regard.

### 5.2.3 Coalescence and impulsive bursty reconnection

The least stable long-wavelength tearing modes ( $\lambda^{\text{max}} \sim L_y$ ) tend to saturate soon after the onset of the nonlinear phase. For efficient reconnection to occur the presence of a significantly strong external driver (e.g. sudden crustal motions at the footpoints of sheared arcades, the onset of an ideal instability, or the catastrophic ejection of a flux rope) may be required, which forces a current sheet to become unstable to shorter wavelength modes ( $\lambda^{\text{max}} \ll L_y$ ), such that a chainlike structure of magnetic islands is formed before the nonlinear phase sets in (Uzdensky & Loureiro 2014). This configuration is consequently unstable to the coalescence instability, whereby the magnetic islands approach each other through mutually attractive Lorentz forces since they essentially comprise parallel flowing current concentrations. Island coalescence is typically subdivided into two phases: (1) the ideal MHD phase, where the current loops approach one another, and (2) the resistive reconnection phase, where due to finite resistivity ( $\eta \neq 0$ ) and large field gradients between the approaching current loops, the loops merge to form one current loop with an increased cross section, i.e. larger magnetic island. Stability analysis was performed by Finn & Kaw (1977) on a particular periodic island-chain configuration described by a Fadeev force-free equilibrium (Fadeev et al. 1965),

$$\begin{aligned}\psi_0 &= \ln[\cosh(kx) + \epsilon \cos(ky)], \\ \mathbf{B}_0 &= B_0 \hat{\mathbf{x}} \times \nabla \psi_0, \\ \nabla^2 \psi_0 &= 4\pi j_{z0} = (1 - \epsilon^2)k^2 \exp[-2\psi_0],\end{aligned}$$

where  $\psi_0$  is the equilibrium magnetic flux function,  $B_0$  the local (background) magnetic field,  $j_{z0}$  the equilibrium current directed perpendicular to the reconnection plane, and  $0 < \epsilon < 1$  the peakedness parameter of the current concentration in the magnetic islands. Subsequent numerical simulations have shown that, for a large range of  $S_\delta$ , the coalescence growth rate is much greater than the tearing growth rate (Pritchett & Wu 1979) and that it depends critically on the value for  $\epsilon$  (Bhattacharjee et al. 1983); linear tearing corresponding to  $\epsilon = 0$ .

The coalescence instability is characterised by two timescales associated with its distinct phases (Kliem 1995). During the ideal phase the current loops approach each other on a hydromagnetic timescale, whereby the length scale is given by the separation distance of paired current loops  $\lambda_C$ ,

$$\tau_{C1} \sim \epsilon^{-1} \frac{\lambda_C}{v_A} \quad (82)$$

with  $\delta \lesssim \lambda_C \lesssim \lambda^{\text{max}}$ . In general  $\tau_{C1} \ll \tau_{\text{tm}}^{\text{min}}$ , yet no magnetic energy is dissipated in the process. During the resistive phase, when the current loops merge, ‘anti-reconnection’ occurs in-between the approaching islands. The reconnection

rate is enhanced by the external driving forces of the converging current loops, such that in general  $\tau_{C2} < \tau_{\text{tm}}^{\text{min}}$ . Moreover, for strongly peaked current concentrations ( $\epsilon \rightarrow 1$ ), we have  $\tau_{C1} \sim \tau_{C2} \ll \tau_{\text{tm}}^{\text{min}}$ . For  $\lambda_C^{\text{max}} \simeq \lambda^{\text{max}} \sim 10^6$  cm, the coalescence timescale becomes comparable to the magnetospheric light crossing time, i.e.  $\tau_C \sim \tau_A^{\text{ext}} \epsilon^{-1}$  ms.

Coalescence following tearing converts the bulk of the free magnetic energy in the current sheet, such that the island growth phase may act as mere prelude to the explosive energy release of merging current loops (Leboeuf et al. 1982). Its rapid development and ability to convert a significant fraction of magnetic energy argue in favour of coalescence, rather than tearing, as an explanation for the impulsive phase of flares (Tajima et al. 1982, 1987; Sakai & Ohsawa 1987; Kliem 1995; Schumacher & Kliem 1997). The observed giant flare emission may therefore be a proxy of the nonlinear, rather than the linear, tearing phase.

Furthermore, for higher values of  $S_\delta$  and  $\sigma_m$  a nonlinear process known as ‘impulsive bursty reconnection’ may occur, whereby a cycle of slow tearing, rapid coalescence, current sheet thinning, and further secondary tearing (i.e. the plasmoid instability) at an increased rate repeats successively (Leboeuf et al. 1982; Priest 1985; Uzdensky et al. 2010). Consequently, energy is released during separate coalescence events in a fragmentary and quasi-periodic manner. This process is advanced to explain the periodic temporal fine structure of hard X-ray (HXR) emission and coherent drifting radio bursts associated with discrete (bidirectional) electron beams observed during the impulsive phase of solar flares (Aschwanden et al. 1995; Kliem et al. 2000; Karlicky 2004). Quasi-periodic oscillations (QPOs) of  $\nu \sim 10^2$  Hz, that might be associated with separate energy injections, have also been detected during the initial phases of the magnetar giant flares: See Subsection 2.2. These distinct energy surges may be interpreted as quasi-periodic peaks in coalescence rates<sup>13</sup>, resulting from impulsive bursty reconnection. Precise timing observations of hypothesised (drifting) radio burst from magnetars (Lyutikov 2002) may greatly help to further probe the reconnection substructure (e.g. separate plasmoids), reconnection rate, and density of the acceleration region. Yet even though various magnetars show radio emission (e.g. Camilo et al. 2006), no such bursts of coherent radio emission coincident with the (recurrent)  $\gamma$ -ray bursts have been observed to date.

The total energy release through a multitude of coalescence events may be estimated accordingly (Krüger et al. 1989; Kliem 1995),

$$U_C^{\text{tot}} \simeq \frac{(N_C - 1)^3}{N_C} \frac{\lambda_C^2 L_z B_0^2}{24\pi^2} \ln\left(\frac{\lambda_C}{\delta}\right), \quad (83)$$

where  $N_C$  is the number of individual coalescence events. If we estimate the total number of coalescence events during the impulsive phase of a giant flares as follows,

$$N_C \simeq \nu \tau_{\text{spike}} \frac{L_y}{\lambda_C^{\text{max}}} \sim 10^2, \quad (84)$$

we find for the total energy release through dynamic current

<sup>13</sup> Quasi-periodic pulsations (QPPs) are ubiquitously observed in solar flares; among self-oscillatory reconnection, a multitude of alternative mechanisms have been proposed to explain these phenomena (Nakariakov & Melnikov 2009).

sheet reconnection,

$$U_C^{\text{tot}} \sim 10^{45} N_{C,2}^2 (\lambda_{C,6}^{\text{max}})^2 L_{z,6} B_{s,15}^2 r_7^{-5} \ln \left( \frac{\lambda_{C,6}^{\text{max}}}{\delta_4} \right) \text{ erg}, \quad (85)$$

where  $L_{z,6} = L_z/10^6$  cm is the length of a current loop. This estimate is consistent with the observed energy output of the initial spike – see Table 1.

## 6 SUMMARY

To better understand the extreme nature of the explosive onset of magnetar giant flares, we have discussed impulsive reconnection through the spontaneous development of the linear tearing instability in a globally sheared external field as a candidate trigger mechanism. Upon reexamination of previous works on the (relativistic) linear tearing mode, we found that the minimum growth time in magnetar magnetospheres is  $\tau_{\text{tm}}^{\text{min}} \sim 10^{-1}$  ms [Eq. (51)]. This estimate is consistent with the typical  $e$ -folding rise times ( $\tau_e \sim 0.1 - 1$  ms) of the giant flare light curves (see Table 1). Our result differs significantly from the one found by Lyutikov (2003) ( $\tau_{\text{tm}}^{\text{L03}} \sim 10$  ms). Even though the rescaling of the current sheet thickness (by a factor of  $10^{-2}$ ) has a larger effect on the final result, the difference is however essentially due to an error in that calculation.

Assuming the validity of the assumption that the exponential rise time of the giant flare is a proxy for the linear growth time of the tearing mode  $\tau_{\text{tm}}^{\text{min}} = \tau_e$ , we obtained order of magnitude estimates for the thickness of the current sheet and height of the base of the reconnection region, respectively  $\delta \sim 10^4$  cm and  $r \sim 10^7$  cm, through elementary pressure balance and energy conservation considerations. Additionally we found that the global length of the current sheet would have to be  $L_y \sim (3 - 10) R_*$ , which is reasonable for the giant flares, yet problematic for the smaller recurrent bursts, since such large unstable regions would have to develop on very short timescales  $\Delta T \sim 100$  s, where  $\Delta T$  represents the typical waiting time of recurrent bursts (Gögüş et al. 1999, 2000).

Finally we discussed the obtained constraints on the reconnection geometry and evaluated the soundness of the aforementioned assumption of equating an MHD growth time with an emission timescale. Regarding the latter, it is not apparent whether linear tearing dictates the rate of radiation release and if during the linear tearing phase magnetic field dissipation occurs efficiently enough to generate the observed emission. Considering the impulsive phase of solar flares there is no unequivocal connection between linear tearing and the observed high energy emission that is ultimately radiated by accelerated nonthermal particles. Moreover, substantial pair production in magnetar magnetospheres may obscure the emission resulting from magnetic field dissipation through reconnection, altogether.

Furthermore, nonlinear effects become significant soon after the onset of linear tearing and in general reduce the reconnection rate considerably. Fast and efficient reconnection during the nonlinear impulsive bursty regime that may follow tearing, requires however the presence of a strong external driver e.g. rapid crustal motion or catastrophic loss of equilibrium of external magnetic field configurations. Accordingly, we propose that future research into

magnetospheric trigger mechanisms for magnetar (giant) bursts investigate *driven* reconnection scenarios, where the emission timescales may constrain the development of the external driver, the nonlinear reconnection phase, or the intense reconnection aftereffects.

**Acknowledgments:** C.E. acknowledges support from NOVA (Nederlandse Onderzoeksschool voor Astronomie). A.W. acknowledges support from NWO Vidi Grant 639.042.916. The work of R.T. is partially supported by INAF through a PRIN grant. J.H. is supported by the Natural Sciences and Engineering Research Council of Canada. We would like to thank Sam Lander, Lyndsay Fletcher, Maxim Lyutikov, Serguei Komissarov, and the participants of the ‘Integrated Plasma Modelling of Solar Flares’ Lorentz Center workshop (May 2015) for helpful discussions. We also wish to acknowledge the useful and significant feedback from the anonymous referees.

## REFERENCES

- Aschwanden M.J., Benz A.O., Dennis B.R., et al., 1995, *ApJ*, 455, 347
- Aschwanden M.J., 2006, *Physics of the Solar Corona* (Springer & Praxis Publishing Ltd, Chichester, UK)
- Barat C., Hayles R.I., Hurley K., et al., 1983, *A&A*, 126, 400
- Beloborodov A.M., Thompson C., 2007, *ApJ*, 657, 967
- Beloborodov A.M., 2009, *ApJ*, 703, 1044
- Bhattacharjee A., Brunel F., Tajima T., 1983, *Phys. of Fluids*, 26, 3332
- Bibby J.L., Crowther P.A., Furness J.P., Clark J.S., 2008, *MNRAS*, 386, L23
- Blaes O., Blandford R., Goldreich P., Madau P., 1989, *ApJ*, 343, 839
- Braithwaite J., Spruit H.C., 2006, *A&A*, 450, 1097
- Braithwaite J., 2009, *MNRAS*, 397, 763
- Camilo F., Ransom S.M., Halpern J.P., et al., 2006, *Nature*, 442, 892
- Cerutti B., Werner G.R., Uzdensky D.A., Begelman M.C., 2014, *ApJ*, 782, 104
- Ciolfi R., Rezzolla L., 2013, *MNRAS*, 435, L43
- Cline T.L., Desai U.D., Pizzichini G., et al., 1980, *ApJ*, 237, L1
- Davies B., Figer D.F., Kudritzki R.-P., et al., 2009, *ApJ*, 707, 844
- Duncan R.C., 2004, In: Höflich P., Kumar P., Wheeler J.C., 2004, (eds.) *Cosmic Explosions in Three Dimensions*, (Cambridge, UK: Cambridge Univ. Press)
- Egedal J., Daughton W., Le A., 2012, *Nature Phys. Lett.*, 8, 321
- Fadeev V.M., Kvabtskhava I.F., Komarov N.N., 1965, *Nucl. Fusion*, 5, 202
- Fenimore E.E., Klebesadel R.W., Laros J.G., 1996, *ApJ*, 460, 964
- Feroci M., Hurley K., Duncan R.C., Thompson C., 2001, *ApJ*, 549, 1021
- Ferrario L., Wickramasinghe D., 2006, *MNRAS*, 367, 1323
- Finn J.M., Kaw P.K., 1977, 20, 72
- Fletcher L., Hudson H.S., 2008, *ApJ*, 675, 1645
- Flowers E., Ruderman M.A., 1977, *ApJ*, 215, 302
- Furth H.P., Killeen J., Rosenbluth M.N., 1963, *Phys. of Fluids*, 6, 459
- Gavriil F.P., Kaspi V.M., Woods P.M., 2004, *ApJ*, 607, 959
- Gedalin M., 1996, *Phys. Rev. Lett.*, 76, 3340
- Gill R., Heyl J., 2010, *MNRAS*, 407, 1926
- Goedbloed J.P., Keppens R., Poedts S., 2009, *Advanced Magnetohydrodynamics* (Cambridge: Cambridge Univ. Press)

- Gögüş E., Woods P.M., Kouveliotou C., et al., 1999, *ApJ*, 526, L93
- Gögüş E., Woods P.M., Kouveliotou C., et al., 2000, *ApJ*, 532, L121
- Gögüş E., Kouveliotou C., Woods P.M., et al., 2001, *ApJ*, 558, 228
- Goldreich P., Reisenegger A., 1992, *ApJ*, 395, 250
- Goldston R.J., Rutherford P.H., 1995, *Introduction to Plasma Physics*. CRC Press.
- Gourgouliatos K.N., Cumming A., 2014, *Phys. Rev. Lett.*, 112, 171101
- Harding A.K., Lai D., 2009, *Rep. Prog. Phys.*, 69, 2631
- Haschke R., Grebel E.K., Duffau S., 2012, *ApJ*, 144, 107
- Henriksson K.T., Wasserman I., 2013, *MNRAS*, 431, 2986
- Heyl J.S., Kulkarni S.R., 1998, *ApJ*, 506, L61
- Hoffman K., Heyl J., 2012, *MNRAS*, 426, 2404
- Horowitz C.J., Kadav K., 2009, *Phys. Rev. Lett.*, 102, 191102
- Hoshino M., Lyubarsky Y., 2012, *Space Sci. Rev.*, 173, 521
- Huang L., Yu C., 2014, *ApJ*, 784, 168
- Huang L., Yu C., 2014, *ApJ*, 796, 3
- Hurley K., Cline T., Mazets E., et al., 1999, *Nature*, 397, 41
- Hurley K., Boggs S.E., Smith D.M., et al., 2005, *Nature*, 434, 1098
- Jones P.B., 2003, *ApJ*, 595, 342
- Kagan D., Milosavljevic M., Spitkovsky A., 2013, *ApJ*, 774, 41
- Karlicky M., 2004, *A&A*, 417, 325
- Kliem B., 1995, *Proc-1995-Benz*, 93
- Kliem B., Karlicky M., Benz A.O., 2000, *A&A*, 360, 715
- Komissarov S.S., 2002, *MNRAS*, 336, 759
- Komissarov S.S., Barkov M., Lyutikov M., 2007, *MNRAS*, 374, 415 (KBL07)
- Krüger A., Kliem B., Hildebrandt J., 1989, *ESA-SP*, 285, 169
- Lander S.K., Jones D.I., 2012, *MNRAS*, 424, 482
- Lander S.K., 2014, *MNRAS*, 437, 424
- Lander S.K., Andersson N., Antonopoulou D., et al., 2015, *MNRAS*, 449, 2047
- Leboeuf J.N., Tajima T., Dawson J.M., 1982, *Phys. of Fluids*, 25, 784
- Levin Y., Lyutikov M., 2012, *MNRAS*, 427, 1574
- Link B., 2014, *MNRAS*, 441, 2676
- Liu W., Petrosian V., Dennis B.R., Jiang Y.W., 2008, *ApJ*, 676, 704
- Liu S., Fletcher L., 2009, *ApJ*, 701, L34
- Low B.C., 1973, *ApJ*, 181, 209
- Lyutikov M., 2002, *ApJ*, 580, L65
- Lyutikov M., 2003, *MNRAS*, 346, 540 (L03)
- Lyutikov M., 2006, *MNRAS*, 367, 1594
- Masada Y., Nagataki S., Shibata K., Terasawa T., 2010, *PASJ*, 62, 1093
- Mazets E.P., Golenetskii S.V., Il'Inskii V.N., et al., 1979, *Nature*, 282, 587
- Mazets E.P., Golenetskii S.V., 1981, *Astrophys. & Space Sci.*, 75, 47
- Mazets ., Cline ., Aptekar ., et al., 1999, *Astron. Lett.*, 25, 635
- Mereghetti S., Tiengo A., Esposito P., et al., 2005, *ApJ*, 628, 938
- Mereghetti S., Esposito P., Tiengo A., et al., 2006, *ApJ*, 653, 1423
- Mereghetti S., 2008, *A&A Rev.*, 15, 225
- Mikić Z., Linker J.A., 1994, *ApJ*, 430, 898
- Nakagawa Y.E., Mihara T., Yoshida A., et al., 2009, *Astron. Soc. of Japan*, 61, 387
- Nakariakov V.M., Melnikov V.F., 2009, *Space Sci. Rev.*, 149, 119
- Narukage N., Shibata K., 2006, *ApJ*, 637, 1122
- Olausen S.A., Kaspi V.M., 2014, *ApJSuppl. Series*, 212, 6
- Palmer D.M., Barthelmy S., Gehrels N., et al., 2005, *Nature*, 434, 1107
- Parfrey K., Beloborodov A.M., Hui L., 2013, *ApJ*, 774, 92
- Petrosian V., Liu S.M., 2004, *ApJ*, 610, 550
- Priest E.R., 1985, *IAU Symposia*, 107, 233
- Priest E., Forbes T., 2000, *Magnetic Reconnection: MHD Theory and Applications* (New York: Cambridge Univ. Press)
- Pritchett P.L., Wu C.C., 1979, *Phys. of Fluids*, 22, 2140
- Pucci F., Velli M., 2013, *ApJ*, 780, L19
- Rea N., Tiengo A., Mereghetti S., et al., 2005, *ApJ*, 627, L133
- Rutherford P.H., 1973, *Phys. of Fluids*, 16, 1903
- Sakai J.I., Ohsawa Y., 1987, *Space Sci. Rev.*, 46, 113
- Schumacher J., Kliem B., 1997, *Phys. of Plasmas*, 4, 3533
- Schwartz S.J., Zane S., Wilson R.J., et al., 2005, *ApJ*, 627, L129
- Shibata K., Tanuma S., 2001, *Earth Planets Space*, 53, 473
- Shibata K., Magara T., 2011, *Living Rev. in Solar Phys.*, 8, 6
- Sironi L., Spitkovsky A., 2014, *ApJ*, 783, L21
- Speiser T.W., 1965, *J. of Geophys. Res.*, 70, 4219
- Steinolfson R.S., van Hoven G., 1984, *Phys. of Fluids*, 27, 1207
- Tajima T., Brunel F., Sakai J., 1982, *ApJ*, 258, L45
- Tajima T., Sakai J., Nakajima H., et al., 1987, *ApJ*, 321, 1031
- Tanaka Y.T., Terasawa T., Kawai N., et al., 2007, *ApJ*, 665, L55
- Terasawa T., Tanaka Y.T., Takei Y., et al., 2005, *Nature*, 434, 1110
- Thompson C., Duncan R.C., 1992, *ApJ*, 392, L9
- Thompson C., Duncan R.C., 1995, *MNRAS*, 275, 255
- Thompson C., Duncan R.C., 1996, *ApJ*, 473, 322
- Thompson C., Duncan R.C., 2001, *ApJ*, 561, 980
- Thompson C., Lyutikov M., Kulkarni S.R., 2002, *ApJ*, 574, 332
- Tiengo A., Esposito P., Mereghetti S., et al., 2009, *MNRAS*, 399, L74
- Turolla R., Zane S., Watts A., 2015, *Rep. on Progress in Phys.*, 73, 116901
- Uchida T., 1997, *Phys. Rev. E*, 56, 2181
- Uzdensky D.A., Loureiro N.F., Schekochihin A.A., et al., 2010, *Phys. Rev. Lett.*, 105, 235002
- Uzdensky D.A., 2011, *Space Sci. Rev.*, 160, 45
- Uzdensky D.A., Loureiro N.F., 2014, *arXiv: 1411.4295*
- White R.B., 1986, *Rev. Mod. Phys.*, 58, 183
- Wolfson R., 1995, *ApJ*, 443, 810
- Woods P.M., Kouveliotou C., van Paradijs J., et al., 1999, *ApJ*, 518, L103
- Woods P.M., Kouveliotou C., Gögüş E., et al., 2001, *ApJ*, 552, 748
- Yu C., 2012, *ApJ*, 757, 67
- Yu C., 2013, *ApJ*, 771, L46
- Zenitani S., Hoshino M., 2001, *ApJ*, 562, L63
- Zenitani S., Hoshino M., 2007, *ApJ*, 670, 702
- Zenitani S., Hoshino M., 2008, *ApJ*, 677, 530